Journal of Molecular Structure 1189 (2019) 57–65

Contents lists available at ScienceDirect

Journal of Molecular Structure

journal homepage: http://www.elsevier.com/locate/molstruc

Cytotoxicity and antibacterial activities of plant-mediated synthesized zinc oxide (ZnO) nanoparticles using *Punica granatum* (pomegranate) fruit peels extract

Siti Nur Amalina Mohamad Sukri [a], Kamyar Shameli [a, *], Magdelyn Mei-Theng Wong [b], Sin-Yeang Teow [b], Jactty Chew [c], Nur Afini Ismail [a]

[a] Malaysia-Japan International Institute of Technology, Universiti Teknologi Malaysia, Jalan Sultan Yahya Petra, 54100, Kuala Lumpur, Malaysia
[b] Department of Medical Sciences, School of Healthcare and Medical Sciences, Sunway University, Jalan Universiti, Bandar Sunway, 47500 Selangor Darul Ehsan, Malaysia
[c] Department of Biological Sciences, School of Science and Technology, Sunway University, Jalan Bandar Sunway, 47500, Selangor Darul Ehsan, Malaysia

ARTICLE INFO

Article history:
Received 7 February 2019
Received in revised form
3 April 2019
Accepted 5 April 2019
Available online 6 April 2019

Keywords:
Zinc oxide nanoparticles
Punica granatum
Antibacterial applications
Cytotoxicity assay
Transmission electron microscopy

ABSTRACT

The unique properties of zinc oxide nanoparticles (ZnO-NPs) produced using plant extract make them attractive for use in medical as well as industrial applications, and it is necessary to develop environmentally friendly methods for their synthesis. This can be accomplished by replacing the traditional chemical compounds for the reduction of the zinc ions to ZnO-NPs during synthesis with natural plant extracts. Here, the biosynthesis of ZnO-NPs using *Punica granatum* (*P. granatum*) fruit peels extract was investigated as the reducing and stabilizing agent. The *P. granatum*/ZnO-NPs with spherical and hexagonal shapes were biosynthesized at different annealing temperatures. The X-ray diffraction analysis confirmed the synthesis of highly pure ZnO-NPs with increasing crystallinity in higher annealing temperatures. The ZnO-NPs displayed characteristic absorption peaks between 370 and 378 nm in the UV−vis spectra. Transmission electron microscopy (TEM) imaging showed the formation of mostly spherical and hexagonal-shaped ZnO-NPs in the mean size of 32.98 nm and 81.84 nm at 600 °C and 700 °C respectively. According to FTIR spectrum, strong absorption bands in the range of 462–487 cm^{-1} corresponding to Zn−O bond stretching can be seen. Antibacterial activities of *P. granatum*/ZnO-NPs against *Escherichia coli* (*E. coli*) and *Enterococcus faecalis* (*E. faecalis*) were investigated and compared. Results obtained show that smaller-sized *P. granatum*/ZnO-NPs are more effective in inhibiting growth of both bacteria. In addition, cytotoxicity assays were performed for *P. granatum*/ZnO-NPs against human colon normal and cancerous cells. *P. granatum*/ZnO-NPs exhibited similar killing activities of both cell lines at the concentration of ≥31.25 μg/mL. The biosynthesized ZnO-NPs could offer potential applications in biomedical field.

1. Introduction

The field of nanotechnology has been constantly growing as researchers explore more about novel materials in nanoscale level [1]. Nanotechnology provides the platform for construction of novel nanostructures, understanding their novel properties, and learning how to make use of them in different field of applications [2]. Nanoparticles are generally synthesized in the range of 1–100 nm and can be produced from many metal compounds like silver, gold, zinc, copper, iron, titanium, etc., by various physical and chemical methods [3]. Even though synthesis of nanoparticles can be carried out by any method, green synthesis has gained prominence in recent years [4]. Compared to traditional chemical or physical methods, green synthesis method in synthesizing nanoparticles offers many advantages, such as requires mild reaction conditions, uses less toxic chemicals, is inexpensive and ecofriendly [5]. The green synthesis method utilizes a variety of biological agents, including plant extracts, fruit extracts, microbes, and others [6].

Zinc oxide (ZnO) is a semiconductor with a large band gap of about 3.37 eV [7] and high exciton binding energy (60 meV) [8]. It is a multifunctional compound with unique optic, luminescent,

* Corresponding author.
E-mail address: kamyarshameli@gmail.com (K. Shameli).

https://doi.org/10.1016/j.molstruc.2019.04.026
0022-2860/

electronic and optoelectronic properties [8]. Numerous methods including precipitation technique [9], microwave decomposition [10], hydrothermal process [11], wet chemical method [12] and sol-gel method [13] have been adopted to produce ZnO nanoparticles (NPs) with different morphologies and characteristics. Studies have reported the production of ZnO-NPs in different forms like flower-shaped [14], spherical [15], cubic [16], rice-shaped [10] and nanorods [17]. ZnO-NPs synthesis from diverse resources such as *Zizi-phus nummularia* leaf extract [5], starch [18], *gum tragacanth* [13], *Catharanthus roseus* leaf extract [19], honey [7], brown microalga [20] and seaweed [21] have been described previously. The properties of ZnO-NPs have been investigated in a wide range of targeted applications including electrical property [22], antibacterial activity [23], antifungal activity [14], catalytic activity [15] and cosmetic industry [21].

Presently, the problem of antimicrobial resistance (AMR) has reached a critical level and is becoming a global concern. Emergence of antibiotic-resistant microorganisms or 'superbugs' complicates the treatment of bacterial infections, as superbugs restrict the treatment options available to infected individuals. The antibacterial potential of ZnO-NPs has been explored continuously by scholars, in hope to combat bacterial infections, including those caused by superbugs. ZnO-NPs have the ability to inhibit bacterial growth and biofilm formation by inducing oxidative stress that can irreversibly damage cell membrane, DNA as well as mitochondria leading to apoptosis [24]. In 2016, Ghasemi and Jalal in their publication also investigated the synergistic effects of ZnO-NPs with conventional antibiotics against resistant *Acinetobacter baumannii* [25] and reported that the uptake of antibiotics into bacterial cell increased with the addition of ZnO-NPs [25].

Besides its excellent antibacterial properties, ZnO-NPs have been cited in several publications for having anticancer activities [12,15]. ZnO-NPs kill cancerous cells with similar mechanism they eradicate bacterial cells, which is the generation of reactive oxygen species to induce apoptosis [26]. Selective toxicity of ZnO-NPs towards a variety of normal and cancer cell lines have shown intriguing results and the NPs can be developed for use in future cancer therapy [27–29]. By understanding cytotoxicity of ZnO-NPs, we can also determine its possible usage as antimicrobial agents.

Punica granatum fruit (*P. granatum* F.) or pomegranate has been described as a power fruit, well known for its superior therapeutic properties and health benefits to consumers [23]. *P. granatum* F. peel makes up about one third of the fruit and remains as a byproduct after consumption. The usage of these agro-wastes from fruits has acquired significant attention in recent years due to their availability and cost-effectiveness [30]. *P. granatum* F. peel has been well acknowledged for containing extraordinarily high number of phenolic compounds as sources of natural antioxidants [31]. As previously reported, some major phenolic compounds identified in pomegranate peel include punicalagin, gallic acid, ellagic acid, chlorogenic acid, caffeic acid, punicalin, apigenin, quercetin, pelargonidin, cyanidin, granatin A and granatin B [31]. These compounds are primarily concentrated in the peel portion of *P. granatum* and have been proven to aid in green synthesis of a wide range of different NPs [16,32,33].

The present research area defines the *P. granatum* F. peels extract as reducing and stabilizing agents to biosynthesize ZnO-NPs using green synthesis method. ZnO-NPs were successfully synthesized by thermal decomposition in different annealing temperatures. The aim of this work was to employ a simple method for novel biosynthesis of ZnO-NPs and investigate their physicochemical properties. Antibacterial activity of ZnO-NPs was carried out against Gram-positive and Gram-negative bacteria. Cytotoxicity assay of *P. granatum*/ZnO-NPs was investigated for the normal and cancerous cells.

2. Experimental

2.1. Plant collection and materials

The *P. granatum* F. peels were obtained from "Green Farm" in Fars province, city of Neyriz, Iran. Metal salt precursor of analytical grade, zinc nitrate hexahydrate ($Zn(NO_3)_2.6H_2O$, 98%) was purchased from R&M Chemicals, United Kingdom. One Gram-positive (*Enterococcus faecalis* – ATCC 33,186) and one Gram-negative (*Escherichia coli* – MTCC 710,859) bacterial species were used in the antibacterial study. Imipenem antibiotic was purchased from GoldBio (USA). Sterile Mueller-Hinton agar and broth (Becton Dickinson, USA) were used to culture the bacterial strains. 96-well plates for antibacterial application were purchased from Nest Biotech Co., Ltd, China. All aqueous solutions were prepared using deionized (DI) water. Glassware used in this study were thoroughly cleaned with DI water and dried before use.

2.2. Fruit peel extract preparation

Fresh *P. granatum* F. peels were washed thoroughly with tap water to remove dirt and washed again with DI water before dried in the oven at 45 °C. The dried peels were ground using an electric blender into fine powder and stored at room temperature for further use. To produce *P. granatum* F. peel extract, the peel powder was extracted in DI water at 65 °C for 60 min in the ratio of 1:10. The extract were then filtered using mesh to remove large particles and further centrifuged at 10,000 rpm for 10 min to completely eliminate leftover fine sediments. The *P. granatum* F. peel extract was kept at 4 °C for future experiments.

2.3. Synthesis of P. granatum/ZnO–NPs

A simple sol-gel and combustion method was used to synthesize *P. granatum*/ZnO-NPs. Under vigorous stirring at 90 °C, zinc nitrate hexahydrate ($Zn(NO_3)_2.6H_2O$) was added to *P. granatum* F. peel extract in the ratio of 1:10. The solution was stirred until the aqueous solvent is completely removed, leaving a gel-like product. The product was then annealed at different temperatures (400 °C, 500 °C, 600 °C and 700 °C) for 60 min until it turned into fine powder form. The white coloured *P. granatum*/ZnO-NPs powder were then stored in room temperature at about 25 °C for future experiments.

2.4. Characterization methods and instrumentation

The successful production of *P. granatum*/ZnO-NPs was characterized by the use of ultraviolet–visible (UV 1800, SHIMADZU) spectroscopy (UV–vis) in the range of 300 nm–700 nm to observe their absorption peaks. Clean quartz solution cells were used for analysis of each sample. The sample of known concentration in solution form and a blank sample of the solvent (DI water) were used to carry out the experiments. Before placed into the UV–vis chamber, all samples were homogenized in the quartz solution cells. The same instrument was also used to obtain diffuse reflectance spectra of *P. granatum*/ZnO-NPs samples. To evaluate the structures of ZnO-NPs, X-ray diffraction (XRD, Philips, X'pert, Cu Ka) at the small angle range of 2Θ (10 °–90°) was used. Transmission electron microscopy (TEM) (model JEM-2100 F) was used to find the electron diffraction pattern of *P. granatum*/ZnO-NPs and structural analysis of the NPs was performed using FESEM (model JSM 7600 F FESEM). FTIR spectrum was utilized to identify the functional groups present in the biosynthesized NPs. In this study, potassium bromide (KBr) method was used to prepare the tablet containing ZnO-NPs while attenuated total reflection (ATR) method

was adopted to observe absorption peaks in *P. granatum* F. peel extract. The FTIR spectrum was set to run on the range of 400–4000 cm^{-1} using Series 100 FTIR 1650 spectrophotometer (PerkinElmer, Waltham, MA, USA).

2.5. Antimicrobial susceptibility test

Antibacterial properties of *P. granatum*/ZnO-NPs samples were evaluated using broth micro-dilution method based on Clinical and Laboratory Standards Institute (CLSI) protocols. Single colony of Gram-positive (*E. faecalis*) and Gram-negative (*E. coli*) bacteria was isolated from Mueller-Hinton agar (MHA) plates and inoculated into sterile fresh Mueller Hinton broth (MHB). The culture was grown overnight (12–18 h) prior to the experiments. Next day, the bacterial concentration was standardized to an optical density (OD) of 1.0 at 600 nm (approximately 8×10^8 CFU/mL) with MHB. Two-fold serial dilutions of *P. granatum*/ZnO-NPs (S3 and S4) were prepared in 96-well plates to give final test concentrations of 7, 15, 31, 62, 125, 250, 500 and 1000 μg/mL per well. 10 μL of bacterial suspension equivalent to 8×10^6 CFU/mL of exponentially growing bacterial cells were added to the wells. The plates were incubated at 35 ± 2 °C for 18 h. Following the overnight incubation, the plate was then read for the absorbance using microplate reader (GloMax Discover Instrument, Promega) to determine the minimum inhibitory concentrations that prevented 50% growth of the isolates, MIC_{50} values. Positive control, imipenem antibiotic (1 μg/mL), and negative controls (blank, without bacterial inoculum) were included in all experiments.

2.6. Cytotoxicity assay

To determine the cellular killing effect of *P. granatum*/ZnO-NPs samples, cell proliferation assay (Promega) was performed according to the manufacturer's instruction with slight modification. Approximately 5000 human colorectal cancer cell line (HCT116) (ATCC CCL-247) and human normal colon cell (CCD112) (ATCC CRL-1541) cells per well (100 μL/well) were seeded onto a 96-well plate and incubated at 37 °C overnight in a 5% CO_2 humidified incubator. Next day, 2-fold serially diluted ZnO-NPs (250, 125, 62.5, 31.25, 15.63, 7.81 and 0 μg/mL) (100 μL/well) were added into the wells and the plate was incubated for 72 h at 37 °C in the 5% CO_2 humidified incubator. Then 20 μL MTS (3-(4, 5-Dimethylthiazol-2-yl)-5-(3-carboxymethoxyphenyl)-2-(4-sulfophenyl)-2H-tetrazolium) reagent (Promega) per well was added into the plate and incubated for additional 3 h at 37 °C in the 5% CO_2 incubator. Optical density (OD) was then measured at 490 nm using a multimode microplate reader (Tecan). The dose-response graph was plotted by calculating the percentage of cell viability using Eq. (1). In addition, the inhibitory concentrations causing 50% cell growth inhibition (IC_{50} values) were also reported. The images of cells treated with the NPs were captured using an inverted microscope attached to a camera system (IM3 Phase contrast, Optika, Italy).

$$\%\ \text{Viability} = \text{OD of sample well (mean)}/\text{OD of control well (mean)}\ X\ 100 \quad (1)$$

3. Results and discussion

P. granatum F. peel extract contains an abundance of phytochemical compounds that play important roles as reducing and stabilizing agents for the successful yield of ZnO-NPs. Amongst all these compounds, punicalagin and gallic acid make up about 73% of *P. granatum* crude extract with a percentage of 41% and 32% respectively [34]. Therefore, it is assumed that punicalagin and

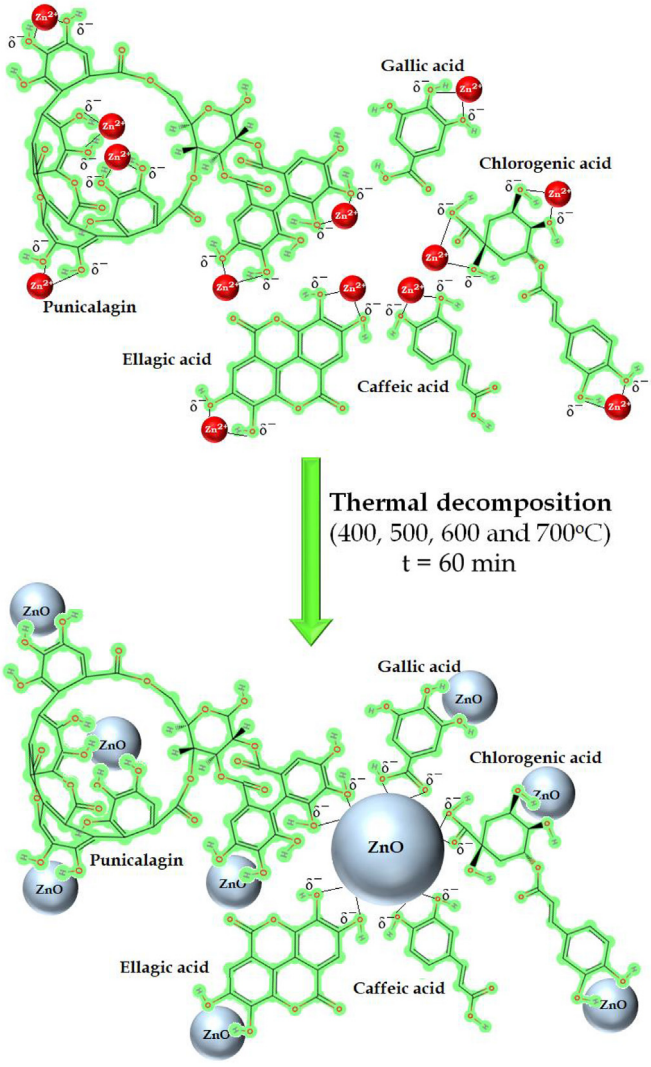

Fig. 1. Schematic diagram of interaction of Zn^{2+} ions with main compounds found in *P. granatum* to produce ZnO-NPs.

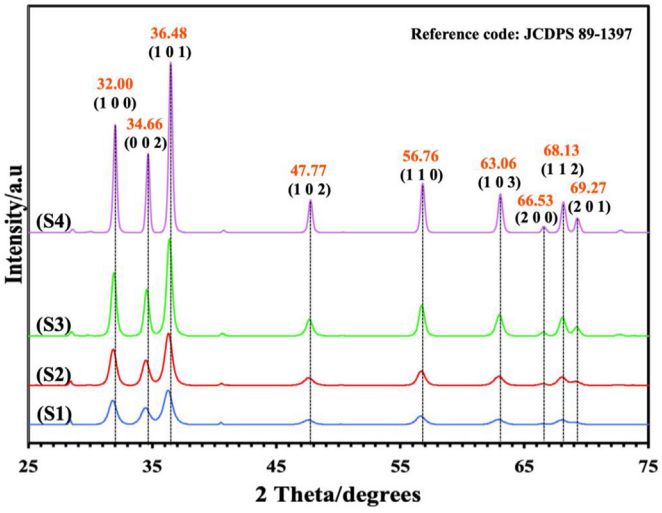

Fig. 2. The XRD of *P. granatum*/ZnO-NPs annealed in 400, 500, 600 and 700 °C (S1–S4), respectively.

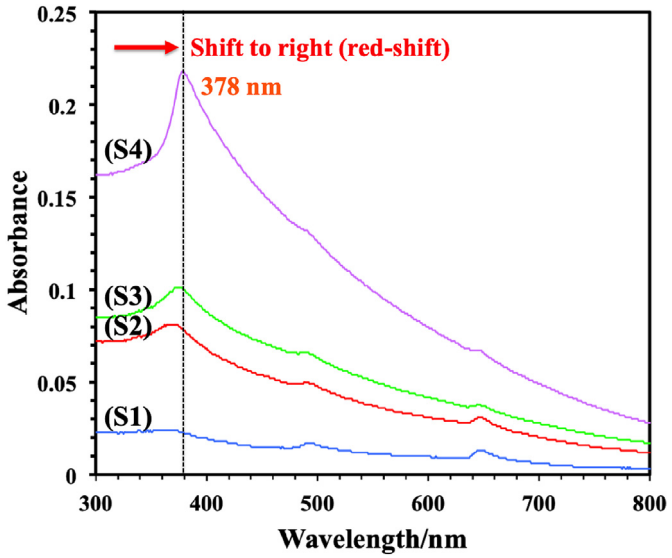

Fig. 3. UV–vis spectra of *P. granatum*/ZnO-NPs annealed in 400, 500, 600 and 700 °C (S1–S4), respectively.

gallic acid majorly contribute in the process of reducing Zn^{2+} ions in the aqueous solution to stable Zn atoms. The possible chemical equations for synthesis of *P. granatum*/ZnO-NPs are shown in Eqs. (2) and (3). Fig. 1 illustrates a possible mechanism of interaction of Zn^{2+} ions and the main compounds of *P. granatum* peel extract. From this illustration, high amounts of negatively charged atoms present in the key compounds donate their electrons and contribute to the stabilization of positively charged Zn^{2+} complex ions. Next, thermal decomposition or annealing process in high temperatures converts the Zn^{2+} complex ions to nano-sized ZnO atoms. In the following discussions, the samples will be referred to as S1, S2, S3 and S4 for *P. granatum*/ZnO-NPs annealed at 400, 500, 600, and 700 °C respectively. The effects of annealing temperature on the NPs production will be investigated and further discussed.

$$P.\,granatum + H_2O_{(L)} + Zn^{+2} \rightarrow [P.\,granatum/Zn^{+2}] \quad (2)$$

$$[P.\,granatum/Zn^{+2}] + O_2 \rightarrow [P.\,granatum/ZnO - NPs] + CO_2\,(g) \quad (3)$$

3.1. X-ray diffraction analysis

The biosynthesis of pure and crystalline *P. granatum*/ZnO-NPs was confirmed using XRD analysis. Miller indices peaks from the analysis are shown in Fig. 2 and can be indexed to hexagonal wurtzite phase structure supported by JCDPS Cardno. 89–1397 data [35]. No other peak related to any foreign compounds is observed in all samples, indicating the *P. granatum*/ZnO-NPs are highly pure. With increasing annealing temperature, a slight shift to the right on all peaks can be observed. The diffraction peaks also become more narrow and intense for S1 until S4. S4 showed most intense diffraction peaks with 2θ values of 32.00°, 34.66°, 36.48°, 47.77°, 56.76°, 63.06°, 66.53°, 68.13° and 69.27° corresponding to the crystal planes of (1 0 0), (0 0 2), (1 0 1), (1 0 2), (1 1 0), (1 0 3), (2 0 0), (1 1 2) and (2 0 1), respectively. This might be caused by improvement in crystallinity for the *P. granatum*/ZnO-NPs when annealed at higher temperature. High temperature supplies enough kinetic energy for the ZnO atoms to migrate to their correct

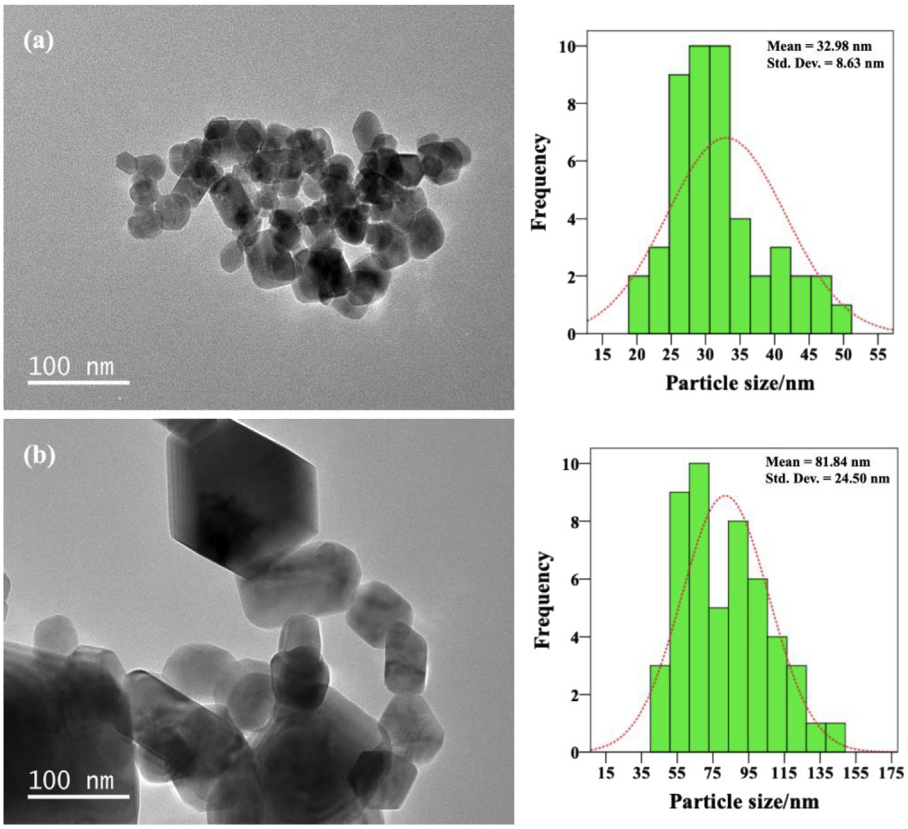

Fig. 4. TEM images of ZnO-NPs at 600 °C and 700 °C (S3–S4) with their respective particle size distribution histograms (a, b).

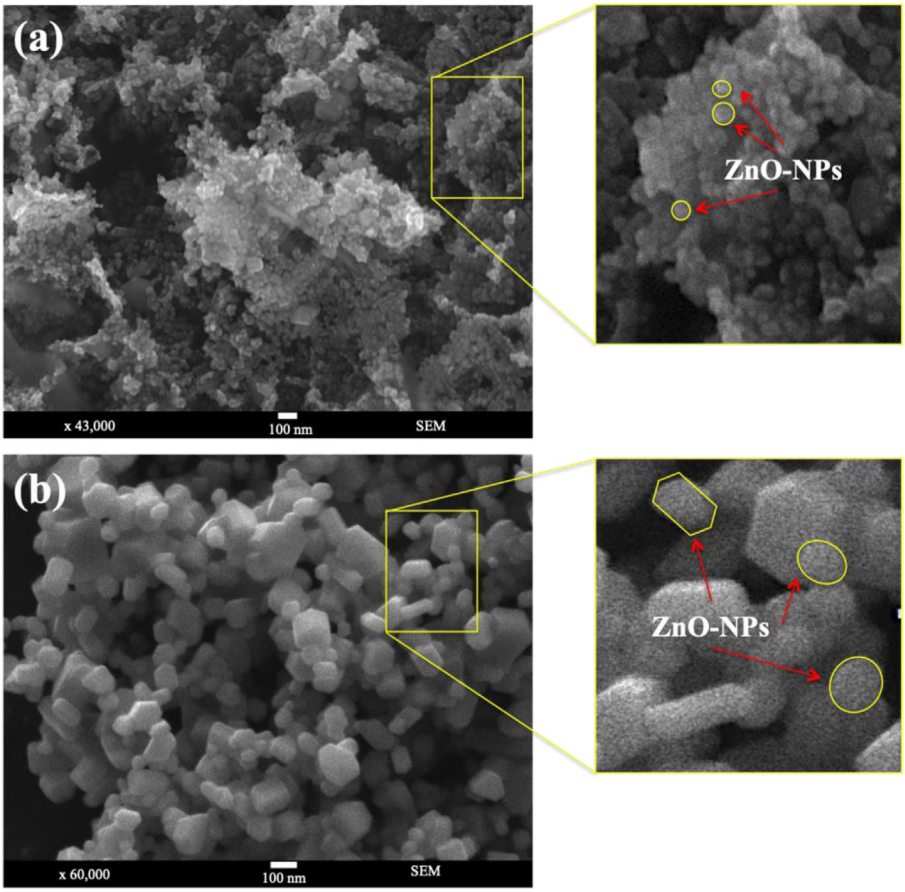

Fig. 5. FESEM images of ZnO-NPs at 600 °C and 700 °C (S3–S4) with their enlarged particle images (a, b).

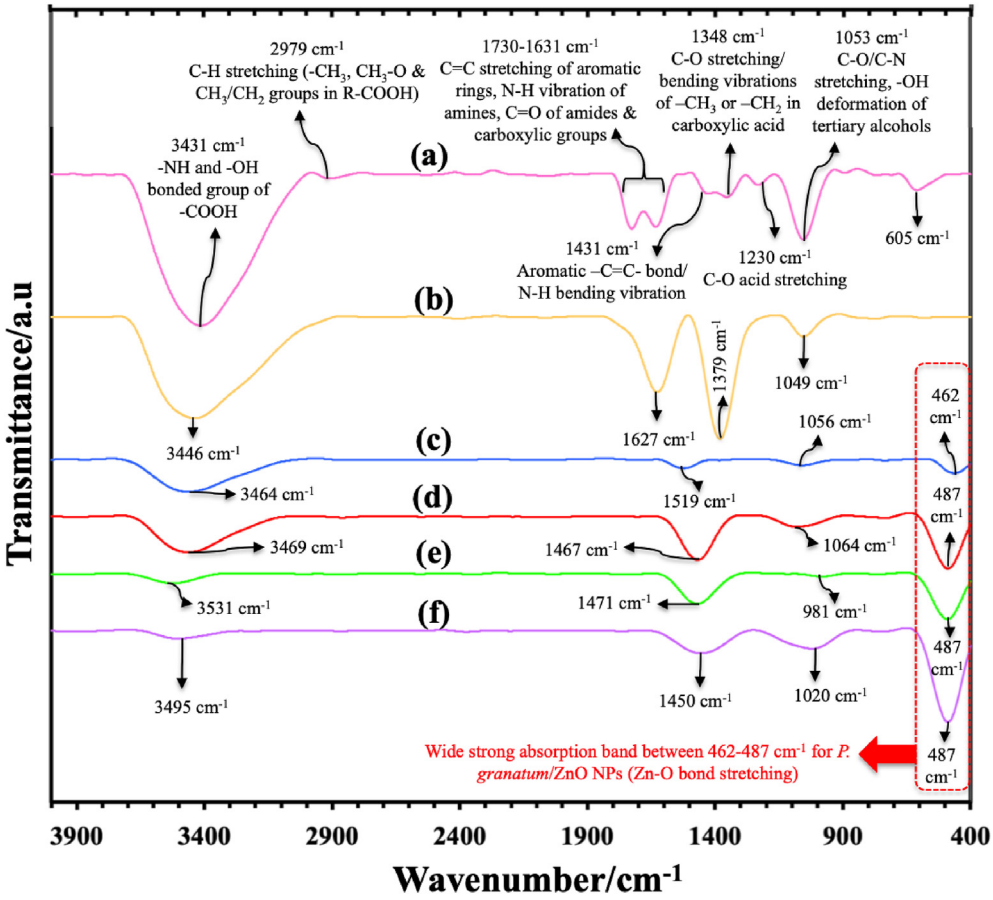

Fig. 6. FTIR spectra of (a) *P. granatum* peel powder, (b) dried gel of P. granatum/$Zn(NO_3)_3.H_2O$, and *P. granatum*/ZnO-NPs annealed at (c) 400 °C: S1, (d) 500 °C: S2, (e) 600 °C: S3, (f) 700 °C: S4.

lattice positions leading to re-crystallization process, reducing defects [36].

The crystallite sizes of S1–S4 can be calculated using the Debye-Scherrer equation, which reveals a relationship between X-ray diffraction peak broadening and crystallite size [37]. The Debye-Scherrer equation is shown below in Eq. (4).

$$d = K\lambda/\beta \cos\theta \quad (4)$$

Based on Eq. (4), d is the average crystallite size of synthesized *P. granatum*/ZnO-NPs, K is the Scherrer constant with a value from 0.9 to 1, λ is the X-ray wavelength (0.154 nm), β is the line broadening in radians, and θ is the Bragg angle. Using Eq. (4), the estimated mean crystallite sizes of ZnO-NPs in S1–S4 were calculated to be 22.39, 30.08, 32.39 and 57.36 nm respectively. Larger *P. granatum*/ZnO-NPs are produced as annealing temperature increases from 400 °C to 700 °C.

3.2. UV–visible (UV–vis) spectroscopy analysis

The production of *P. granatum*/ZnO-NPs was analysed and confirmed by UV–vis spectroscopy in the range of 300–800 nm. The UV–vis spectra displayed excitonic absorption peaks around 370 nm–378 nm for S1 until S4. ZnO's characteristic absorption peak can be detected due to the intrinsic band-gap as excited electrons from its valence band travels to conduction band (O_{2p} => Zn_{3d}) [13]. Based on Fig. 3, from S1 until S4, the peaks become sharper and the wavelength value increases (red shift) as annealing temperature increases due to increase of size of NPs, most probably due to slight agglomeration.

3.3. Morphological studies

TEM imaging was carried out to observe the sizes and structural morphologies of the ZnO-NPs. As shown in Fig. 4a, the shapes of the ZnO-NPs are spherical with slight agglomeration for S3, while hexagonal nanoparticles can also be observed for S4 in Fig. 4b. In correlation with previous discussions of XRD and UV–vis results, it can be witnessed that the sizes of S3 are smaller than that of S4. Particle distribution histograms with normal curve for both samples are plotted and it shows that the average particle sizes of S3 and S4 are 32.98 ± 8.63 and 81.84 ± 24.50 nm, respectively. Based on the particle distribution histograms, it can be determined that higher annealing temperature not only produces bigger nanoparticles but also inconsistent sizes of them. This can be proven by the high standard deviation value of S4 compared to S3 as a wider range of particle sizes can be seen and measured for S4.

FESEM imaging to observe the shapes of S3 and S4 were taken and shown in Fig. 5. Surface topography of the nano-sized ZnO-NPs showed spherical shapes of S3 and also hexagonal shapes for S4, consistent with TEM observations. Meanwhile, NPs of spherical and hexagonal shapes can be observed for S4. From comparison of both images, it is evident that annealing ZnO-NPs at higher temperature produces larger size of NPs, supporting results from XRD, UV–vis and TEM analysis.

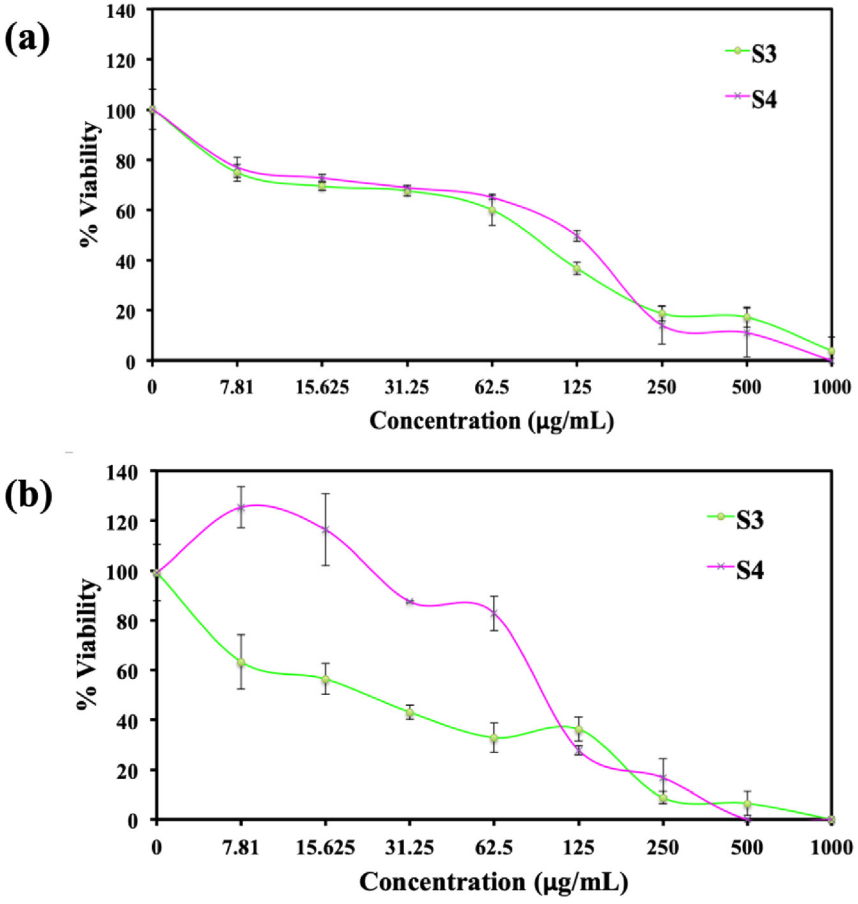

Fig. 7. Percentage viability of (a) *E. coli* and (b) *E. faecalis* in different *P. granatum*/ZnO-NPs concentrations.

3.4. Fourier transform infrared spectroscopy study

The presence of different functional groups in pomegranate peel powder as well as ZnO-NPs before and after annealing process was analysed with FTIR spectroscopy as shown in Fig. 6. Broad peaks can be observed between 3400 cm^{-1} and 3600 cm^{-1} for all samples corresponding to asymmetric and symmetric stretching of H–O–H vibrations (Fig. 6a–f). For S1 until S4, the H–O–H peak slowly disappears with increasing annealing temperatures (Fig. 6c–f). Peak at 3431 cm^{-1} might also originate from bonded –NH and –OH vibrations of –COOH groups found in the *P. granatum* peel powder (Fig. 6a) [38]. The major absorption peaks found in *P. granatum* peel powder can be observed between 1000 cm^{-1} and 1750 cm^{-1} (Fig. 6a). The peak at 1053 cm^{-1} is related to C–O or C–N bond stretching and –OH deformation of tertiary alcohols [39]. In addition, it is assumed that the peak at 1230 cm^{-1} is due to C–O bond stretching of C–O–C or C–O–H groups in *P. granatum* peel [39]. At 1430 cm^{-1}, the absorption peak displayed might be related to aromatic –C=C– bond or N–H bending vibration. Peaks observed at 1631 cm^{-1} and 1730 cm^{-1} possibly refer to C=C stretching of aromatic rings, N–H vibration of amines and C=O stretching of amides and carboxylic groups [39].

Fig. 6b presents the FTIR spectra for dried gel of *P. granatum*/$Zn(NO_3)_3.H_2O$ sample, the complex compound before annealing process into pure *P. granatum*/ZnO-NPs. Medium strength peak can be observed at 1049 cm^{-1} corresponding to C–O bond stretching. Strong peak at 1379 cm^{-1} may refer to C–N stretching amine due to the presence of zinc nitrate metal precursor while the peak at 1627 cm^{-1} corresponds to C=O stretching of functional groups from *P. granatum* F. peel extract. For all ZnO-NPs samples, wide and strong characteristic zinc oxide absorption bands with stretching modes of Zn–O appear around 460 cm^{-1} to 490 cm^{-1} (Fig. 6c–f) [36]. Wide peaks around 1000 cm^{-1} and 1400 cm^{-1} are most likely related to C=O absorption bands due to atmospheric carbon dioxide (CO_2) in the air [40,41].

3.5. Evaluation of antibacterial effects of P. granatum/ZnO-NPs

Line graph plotted as shown in Fig. 7 visualizes the antibacterial activity of *P. granatum*/ZnO-NPs (S3 and S4) in a range of different concentrations. After 18-h incubation of *E. coli* and *E. faecalis* with the samples at 37 °C, absorbance readings were taken and converted into percentage viability using Eq. (1) to measure the growth of both bacteria. Fig. 7a shows a gradual decrease in *E. coli* growth as concentration of S3 and S4 increases. Meanwhile, Fig. 7b demonstrates the inhibition activity of S3 and S4 against *E. faecalis*. The decrease in percentage viability of S4 against *E. faecalis* only occurs after the sample concentration of 31 μg/mL (Fig. 7b). From these results, the minimum inhibitory concentrations that prevents 50% bacterial growth are measured as MIC_{50} and listed in Table 1.

Both samples showed effective antibacterial activities against two strains of bacteria; *E. coli* and *E. faecalis*. S3 showed better antibacterial activities against both bacteria compared to S4 as shown by its lower MIC_{50} values. This might be related to the small particle sizes of S3 that contribute to high amount of active surface area accessible for antibacterial reactions to occur. On the other hand, larger-sized S4 has reduced antibacterial efficacy owing to its lower surface area per volume available to react with the bacterial cells. From literature reviews, it has been agreed that particle size is considered one of the main factors that affect the sensitivity of bacteria towards nanomaterials [14]. Based on several research papers, ZnO-NPs of particle sizes less than 37 nm were successfully synthesized in temperatures lower than 500 °C [38]. MIC value for these ZnO-NPs against *E. coli* and *E. faecalis* were reported to be 32 μg/mL and 16 μg/mL, respectively [42]. Smaller sizes of ZnO-NPs produce lower MIC value as compared to bigger-sized ZnO-NPs.

The exact mechanism of ZnO-NPs killing of bacteria is still being debated and explored, but there are a few proposed antibacterial mechanisms usually discussed among scholars. It is suggested that NPs directly interact with the bacterial cell wall or membrane by releasing metal ions that disrupt the cell permeability, causing damage to the first layer of defence [19]. Upon entry into the cells, the

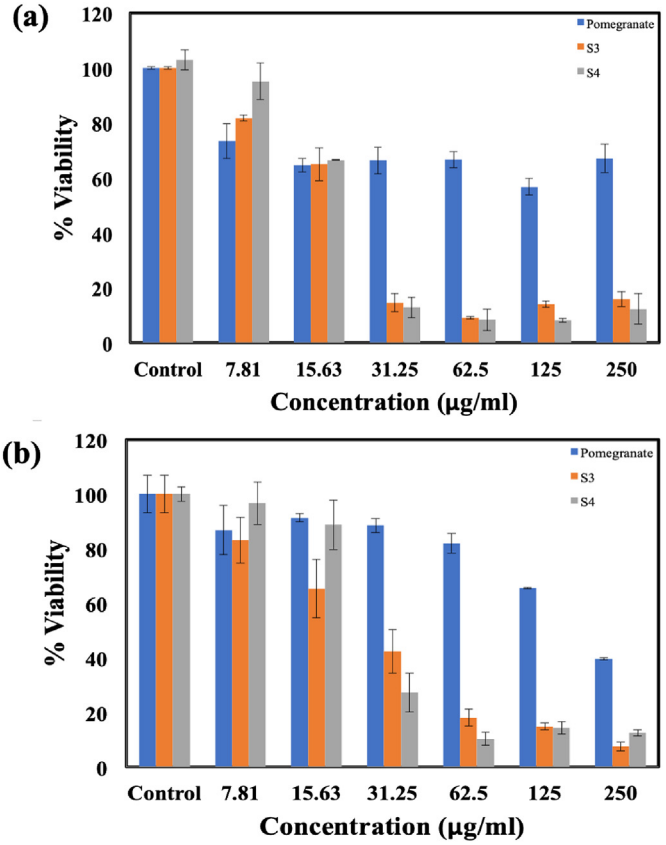

Fig. 8. Anticancer and cytotoxicity effects of pomegranate and *P. granatum*/ZnO-NPs (S3, S4) on (a) colorectal cancer cells (HCT116) and (b) colon normal cells (CCD112) after 72 h of treatment.

Table 1
Minimum inhibitory concentration inhibiting 50% bacterial growth (MIC_{50}) of *P. granatum*/ZnO-NPs samples against *E. coli* and *E. faecalis*.

P. granatum/ZnO-NPs	MIC_{50} (μg/mL)	
	E. coli (Gram-negative)	*E. faecalis* (Gram-positive)
S3	64.53	22.09
S4	90.90	95.21

Table 2
Inhibitory concentration killing 50% cells (IC_{50}) of pomegranate and *P. granatum*/ZnO-NPs (S3, S4) against colorectal cancer cells (HCT116) and normal cell line (CCD112).

P. granatum/ZnO-NPs	IC_{50} (μg/mL)	
	HCT116 (colorectal cancer cells)	CCD112 (normal colon cells)
Pomegranate	96.35	–
S3	28.89	22.12
S4	24.11	17.56

NPs will affect the bacteria's biochemical processes by causing damage to DNA and proteins denaturation [43]. This will finally trigger apoptosis or cell death as the bacteria fails to replicate normally. It can also be noted that Gram-positive bacteria, *E. faecalis* is more susceptible to S3 as lower concentration of S3 (22.09 μg/mL) is needed to inhibit 50% *E. faecalis* growth compared to Gram-negative bacteria, *E. coli*. This finding is similar to previous publications that reported presence of an outer membrane in Gram-negative bacteria might cause them to be more resistant to antimicrobials [44].

3.6. Cytotoxicity and anticancer effects of P granatum/ZnO-NPs

As shown in Fig. 8, the cytotoxicity effects of pomegranate peel powder, S3 and S4 were investigated on CCD112 (normal colon cell line) while anticancer effects were evaluated on HCT116 (colorectal cancer cell line). Pomegranate showed selective toxicity towards colon cancer cells (HCT116) and proved non-toxic to normal cell (CCD112). Cancer cells treated with pomegranate peel powder showed more than 50% decrease in viability (Fig. 8a) at the concentration of 250 μg/mL while normal cells retained their percentage viability (>55%) in all concentrations (Fig. 8b).

Meanwhile, *P. granatum*/ZnO-NPs (S3 and S4) exhibited cytotoxicity against both cell lines as their concentration increased. In cancer cells (Fig. 8a), about 60% killing by S3 was seen at 31.25 μg/mL while approximately 70% killing was observed for S4 at the same concentration. Similarly in normal cells (Fig. 8b), S4 showed slightly higher killing activities (>80%) than S3 at the concentration of 31.25 μg/mL.

Overall, pomegranate showed selective anticancer effects towards cancer cells while S4 demonstrated higher killing activities than S3 against both cells. For all samples, inhibitory concentration killing 50% cells (IC_{50}) were calculated and presented in Table 2. This data is consistent with the microscopic examination as shown in Fig. 9. Unfortunately, these findings suggest that the *P. granatum*/ZnO-NPs tested are not selective enough to be used as anticancer compound as they did not show specificity towards the cancerous cells compared to the normal cells. Thus, further modifications of the NPs are required to improve the NP's specificity.

Fig. 9 displays the microscopic images of normal and sample-treated HCT116 and CCD112 cells for comparison. In the absence of any compound, both cells are in healthy conditions, and are neatly connected with a high concentration of cells in the cell lines [45]. At the concentration of 31.25 μg/mL, pomegranate-treated HCT116 and CCD112 cells show no obvious changes in their structures and morphologies, as the cells remain attached to the wells. In contrast, at the same concentration, S3 and S4-treated HCT116 and CCD112 cells became detached and were dispersed in the wells. This indicates cell deaths due to the cytotoxicity and anticancer effects of *P. granatum*/ZnO-NPs against both cell lines.

4. Conclusions

In this work, *P. granatum* F. peel extract was successfully used to produce ZnO-NPs by acting as reducing and stabilizing agents during the synthesis process. Different annealing temperatures

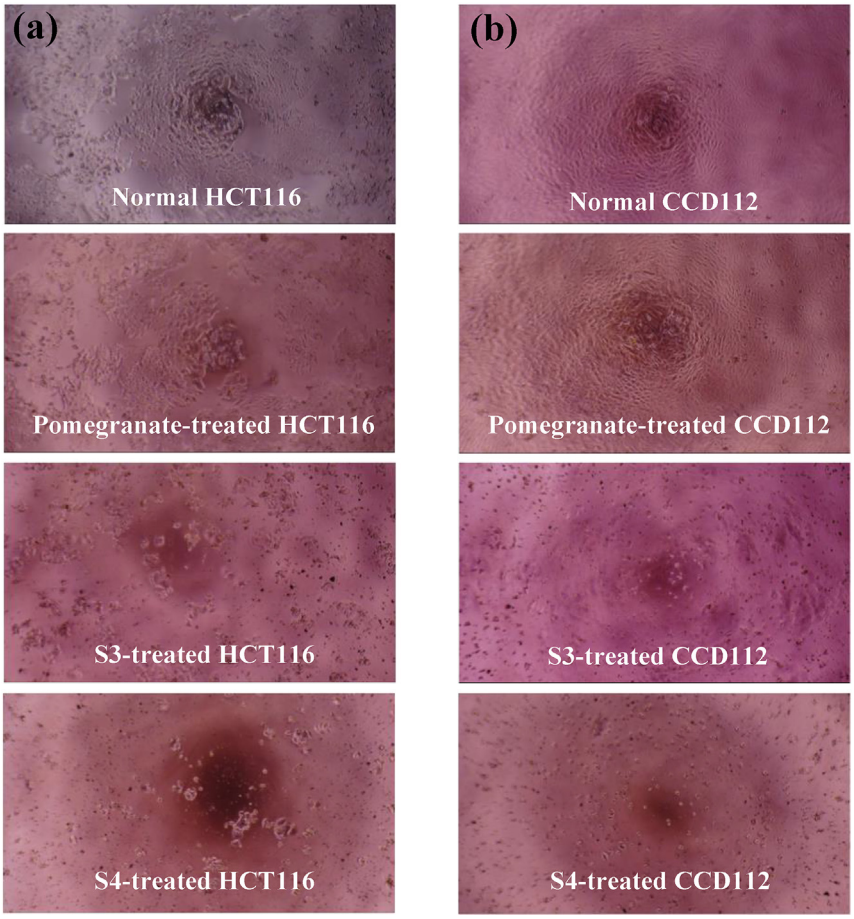

Fig. 9. Microscopic images of untreated, pomegranate-treated, S3-treated and S4-treated (a) colorectal cancer cells, HCT116 and (b) normal colon cells, CCD112 at the sample concentration of 31.25 μg/mL.

between 400 °C to 700 °C were proven to have apparent effects on purity, crystallinity and sizes of *P. granatum*/ZnO-NPs. In higher annealing temperature, pure, highly crystalline and larger-sized *P. granatum*/ZnO-NPs were yielded. These different physicochemical properties dictate the effectiveness of the samples in antibacterial and anticancer applications. Comparative experiments were done using S3 and S4 to analyze their antibacterial and anticancer properties. Smaller-sized S3 of about 32.98 ± 8.63 nm exhibited better inhibition activities against Gram-negative bacteria (*E. coli*) and Gram-positive bacteria (*E. faecalis*) growth. Meanwhile, larger-sized S4 with a mean size of 81.84 ± 24.50 nm was proved to have slightly higher cytotoxicity against both colorectal cancer cells (HCT116) and normal colon cells (CCD112) compared to S3. Further compound modification of the NPs are suggested in order to improve selectivity towards cancerous cells only.

Acknowledgements

The authors wish to acknowledge funding by the Malaysian Ministry of Higher Education under the Tier 1 grants (Grant no. #20H33 and #20H55) and express gratitude to the Research Management Centre (RMC) of Universiti Teknologi Malaysia (UTM) and Malaysia-Japan International Institute of Technology (MJIIT) for providing an excellent research environment and facilities.

Appendix A. Supplementary data

Supplementary data to this article can be found online at https://doi.org/10.1016/j.molstruc.2019.04.026.

References

[1] P. H, S. S, Nanoparticle characterization and application: an overview, Int. J. Current Microbiol. Appl. Sci. 4 (2015) 379–386.
[2] R.G. Saratale, et al., New insights on the green synthesis of metallic nanoparticles using plant and waste biomaterials: current knowledge, their agricultural and environmental applications, Environ. Sci. Pollut. Res. Int. 25 (11) (2018) 10164–10183.
[3] V. K.S, S. R, Plant-based synthesis of nanoparticles and their impact. Nanomaterials in Plants, Algae, and Microorganisms, 2018, pp. 33–57.
[4] R. Sithara, et al., Economical synthesis of silver nanoparticles using leaf extract of Acalypha hispida and its application in the detection of Mn(II) ions, J. Adv. Res. 8 (6) (2017) 561–568.
[5] H. Padalia, S. Chanda, Characterization, antifungal and cytotoxic evaluation of green synthesized zinc oxide nanoparticles using Ziziphus nummularia leaf extract, Artif Cells Nanomed Biotechnol 45 (8) (2017) 1751–1761.
[6] K. Parveen, V. Banse, L. Ledwani, Green Synthesis of Nanoparticles: Their Advantages and Disadvantages, 2016.
[7] S.J. Hoseini, et al., Honey-based synthesis of ZnO nanopowders and their cytotoxicity effects, Adv. Powder Technol. 26 (3) (2015) 991–996.
[8] N.M.A. Hadia, S. García-Granda, J.R. García, Effect of the temperature on structural and optical properties of zinc oxide nanoparticles, J. Nanosci. Nanotechnol. 14 (7) (2014) 5443–5448.
[9] R. Suntako, Effect of zinc oxide nanoparticles synthesized by a precipitation method on mechanical and morphological properties of the CR foam, Bull. Mater. Sci. 38 (4) (2015) 1033–1038.
[10] P. Naresh Kumar, K. Sakthivel, V. Balasubramanian, Microwave assisted biosynthesis of rice shaped ZnO nanoparticles using Amorphophallus konjac tuber extract and its application in dye sensitized solar cells, Mater. Sci.-Poland 35 (1) (2017) 111–119.
[11] N. Lepot, et al., Influence of incorporation of ZnO nanoparticles and biaxial orientation on mechanical and oxygen barrier properties of polypropylene films for food packaging applications, J. Appl. Polym. Sci. 120 (3) (2011) 1616–1623.
[12] M. Premanathan, et al., Selective toxicity of ZnO nanoparticles toward Gram-positive bacteria and cancer cells by apoptosis through lipid peroxidation, Nanomedicine 7 (2) (2011) 184–192.
[13] M. Darroudi, et al., Sol–gel synthesis, characterization, and neurotoxicity effect of zinc oxide nanoparticles using gum tragacanth, Ceram. Int. 39 (8) (2013) 9195–9199.
[14] R. Khan, et al., Flower-shaped ZnO nanoparticles synthesized by a novel approach at near-room temperatures with antibacterial and antifungal properties, Int. J. Nanomed. (2014) 853–864.
[15] N. Elavarasan, et al., Evaluation of photocatalytic activity, antibacterial and cytotoxic effects of green synthesized ZnO nanoparticles by Sechium edule leaf extract, Res. Chem. Intermed. 43 (5) (2016) 3361–3376.
[16] X. Fuku, A. Diallo, M. Maaza, Nanoscaled electrocatalytic optically modulated ZnO nanoparticles through green process of Punica granatumL. And their antibacterial activities, Int. J. Electrochem. (2016) 1–10, 2016.
[17] G. S, et al., Synthesis and characterizations of zinc oxide nanoparticles for antibacterial applications, J. Nanomed. Nanotechnol. (2017) 1–8.
[18] A. Khorsand Zak, et al., Starch-stabilized synthesis of ZnO nanopowders at low temperature and optical properties study, Adv. Powder Technol. 24 (3) (2013) 618–624.
[19] M. Gupta, et al., Effective antimicrobial activity of green ZnO nano particles of Catharanthus roseus, Front. Microbiol. (2018) 1–13.
[20] K. Murugan, et al., Sargassum wightii -synthesized ZnO nanoparticles reduce the fitness and reproduction of the malaria vector Anopheles stephensi and cotton bollworm Helicoverpa armigera, Physiol. Mol. Plant Pathol. 101 (2018) 202–213.
[21] S. Azizi, et al., Green biosynthesis and characterization of zinc oxide nanoparticles using brown marine macroalga Sargassum muticum aqueous extract, Mater. Lett. 116 (2014) 275–277.
[22] T.-T. Liu, et al., Sol–gel synthesis of doped nanocrystalline ZnO powders using xanthan gum and varistor properties study, J. Mater. Sci. Mater. Electron. 26 (11) (2015) 9056–9062.
[23] A. Chaudhary, S. Nandan Rahul, Antibacterial activity of Punica granatum (pomegranate) fruit peel extract against pathogenic and drug resistance bacterial strains, Int. J. Current Microbiol. Appl. Sci. 6 (12) (2017) 3802–3807.
[24] A. Al-Ahmad, et al., Reactive oxygen species mediated bacterial biofilm inhibition via zinc oxide nanoparticles and their statistical determination, PLoS One 9 (11) (2014) 1–9.
[25] F. Ghasemi, R. Jalal, Antimicrobial action of zinc oxide nanoparticles in combination with ciprofloxacin and ceftazidime against multidrug-resistant Acinetobacter baumannii, J Glob Antimicrob Resist 6 (2016) 118–122.
[26] P.K. Mishra, et al., Zinc oxide nanoparticles: a promising nanomaterial for biomedical applications, Drug Discov. Today 22 (12) (2017) 1825–1834.
[27] M. Chandrasekaran, M. Pandurangan, In vitro selective anti-proliferative effect of zinc oxide nanoparticles against Co-cultured C2C12 myoblastoma cancer and 3T3-L1 normal cells, Biol. Trace Elem. Res. 172 (1) (2016) 148–154.
[28] G. Bisht, S. Rayamajhi, ZnO nanoparticles: a promising anticancer agent, Nanobiomedicine 3 (2016) 1–11.
[29] J.W. Rasmussen, et al., Zinc oxide nanoparticles for selective destruction of tumor cells and potential for drug delivery applications, Expert Opin. Drug Deliv. 7 (9) (2010) 1063–1077.
[30] I.A. Adelere, A. Lateef, A novel approach to the green synthesis of metallic nanoparticles: the use of agro-wastes, enzymes, and pigments, Nanotechnol. Rev. 5 (6) (2016) 567–587.
[31] B. Singh, et al., Phenolic compounds as beneficial phytochemicals in pomegranate (Punica granatum L.) peel: a review, Food Chem. 261 (2018) 75–86.
[32] M. Nasiriboroumand, M. Montazer, H. Barani, Preparation and characterization of biocompatible silver nanoparticles using pomegranate peel extract, J. Photochem. Photobiol. B Biol. 179 (2018) 98–104.
[33] S. Phongtongpasuk, S. Poadang, Green synthesis of silver nanoparticles using pomegranate peel extract, Adv. Mater. Res. 1131 (2015) 227–230.
[34] J. Lu, Y. Wei, Q. Yuan, Preparative separation of punicalagin from pomegranate husk by high-speed countercurrent chromatography, J. Chromatogr. B 857 (1) (2007) 175–179.
[35] E. Karaköse, H. Çolak, F. Duman, Green synthesis and antimicrobial activity of ZnO nanostructures Punica granatum shell extract, Green Process. Synth. 6 (3) (2017).
[36] M. Goswami, N.C. Adhikary, S. Bhattacharjee, Effect of annealing temperatures on the structural and optical properties of zinc oxide nanoparticles prepared by chemical precipitation method, Optik 158 (2018) 1006–1015.
[37] V.R. Venu Gopal, S. Kamila, Effect of temperature on the morphology of ZnO nanoparticles: a comparative study, Appl. Nanosci. 7 (3–4) (2017) 75–82.
[38] S. Azizi, et al., Effect of annealing temperature on antimicrobial and structural properties of bio-synthesized zinc oxide nanoparticles using flower extract of Anchusa italica, J. Photochem. Photobiol., B 161 (2016) 441–449.
[39] N. O.R., C. M.M, FTIR analysis and quantification of phenols and flavooids of five commercially available plant extracts used in wound healing, Revista Meteria 21 (3) (2016) 767–779.
[40] N. Shobha, et al., Synthesis and characterization of Zinc oxide nanoparticles utilizing seed source of Ricinus communis and study of its antioxidant, antifungal and anticancer activity, Mater Sci Eng C Mater Biol Appl 97 (2019) 842–850.
[41] A.K. Zak, et al., Effects of annealing temperature on some structural and optical properties of ZnO nanoparticles prepared by a modified sol–gel combustion method, Ceram. Int. 37 (2011) 393–398.
[42] C. Ashajyothi, et al., Antibiofilm activity of biogenic copper and zinc oxide nanoparticles-antimicrobials collegiate against multiple drug resistant bacteria: a nanoscale approach, J. Nanostruct. Chem. 6 (4) (2016) 329–341.
[43] S.A. Khan, et al., Green synthesis of ZnO and Cu-doped ZnO nanoparticles from leaf extracts of Abutilon indicum, Clerodendrum infortunatum, Clerodendrum inerme and investigation of their biological and photocatalytic activities, Mater Sci Eng C Mater Biol Appl 82 (2018) 46–59.
[44] R. Dobrucka, J. Dlugaszewska, M. Kaczmarek, Cytotoxic and antimicrobial effects of biosynthesized ZnO nanoparticles using of Chelidonium majus extract, Biomed. Microdev. 20 (1) (2017) 5.
[45] Z. Izadiyan, et al., Cytotoxicity assay of biosynthesis gold nanoparticles mediated by walnut (Juglans regia) green husk extract, J. Mol. Struct. (2017) 97–105.